Dalton Transactions

Accepted Manuscript

ROYAL SOCIETY OF CHEMISTRY

www.rsc.org/dalton

Journal Name Dalton Transactions Dynamic Article Links ►

Cite this: DOI: 10.1039/c0xx00000x

www.rsc.org/xxxxxx

ARTICLE TYPE

Azide-bridged Cu(II), Mn(II) and Co(II) coordination polymers constructed with a bifunctional ligand of 6-(1H-tetrazol-5-yl)-2,2′-bipyridine

Jung-Yu Tsao, Jia-Dong Tsai and Chen-I Yang*

Received (in XXX, XXX) Xth XXXXXXXXX 20XX, Accepted Xth XXXXXXXXX 20XX
DOI: 10.1039/b000000x

Three new azide-bridged coordination polymers, $[M(N_3)(tzbp)]_n$ (M = Cu, **1·Cu**; Mn, **2·Mn**; Co, **3·Co**), were successfully synthesized by the introduction of a bifunctional tetrazolate/2,2′-bipyridine ligand, 6-(1H-tetrazol-5-yl)-2,2′-bipyridine (Htzbp), from the *in situ* [2+3] cycloaddition of 6-cayno-2,2′-bipyridine in the presence of an excess of sodium azide under hydrothermal conditions. Compounds **1·Cu–3·Co** were characterized by X-ray crystallography, IR spectroscopy, thermogravimetry, and elemental analysis. With $tzbp^-$ ligands acting in the chelating coordination mode, compound **1·Cu** was comprised of a single end-on N_3^- (EO-N_3) bridged one-dimensional (1D) zigzag structure. Both compounds **2·Mn** and **3·Co** adopt two-dimensional (2D) layered structures composed of a double EO-N_3 bridged dinuclear motif, $[M_2(EO\text{-}N_3)_2]$, which are interlinked by $tzbp^-$ ligands in the chelating/bridging mode. The layers of **2·Mn** and **3·Co** are stacked on each other in ···ABAB··· and ···AAAA··· fashions, respectively. Magnetic investigations revealed that intrachain antiferromagnetic interactions were dominant in compound **1·Cu**, and both **2·Mn** and **3·Co** exhibited spin-canted antiferromagnetism behaviour with critical temperatures (T_N) of 3.0 and 18.4 K, respectively. Furthermore, below T_N, the field-induced magnetic transitions of spin-flop and metamagnetism were observed in **2·Mn** and **3·Co**, respectively.

Introduction

The design and synthesis of new coordination polymers (CPs) with paramagnetic metal ions that function as molecule-based magnets have attracted considerable attention and play important roles over recent years.[1-3] Great progress has been made in our understanding of structure–property relationships, such as magneto-structural correlation, of molecular magnetic systems and constructing new magnetic materials with potential technological applications.[4] Enormous efforts in this field have been focused on the design of suitable organic ligands and the ease of coordination of metal ions for the construction of various extended networks.

A variety of short bridging groups, such as azide[5] carboxlate,[6] and five-membered heterocyclic azoles,[7] have been widely studied due to their versatility in both structural and magnetic aspects. They not only connect metal ions in various bridging modes with various dimensionality/topology, but also induce the magnetic exchange of different magnitudes and natures (ferromagnetic, FM, or antiferromagnetic, AF) leading to development of unusual magnetic properties, such as long-range magnetic ordering, metamagnetism, single-molecule magnets (SMMs), and single-chain magnets (SCMs).[8,9] In addition, the rich structural and magnetic diversities of these magnetic systems can be evoked by introduction of different auxiliary organic co-ligands and/or ligands that contain short bridging groups as backbones. Encouraged by the success with tetrazolate-based ligands, a combination of two dissimilar groups as simultaneous bridges has been attempted in pursuit of new magnetic Cps.[10]

In our previous studies, we designed a bridging ligand, 6,6′-bis(1H-tetrazol-5-yl)-2,2′-bipyridine (H_2btzbp), by the unitization of two tetrazolates at the terminal of a 2,2′-bipyridine for the construction of a Co(II) metamagnet.[11] The designed $btzbp^{2-}$ ligand features a chelating/bridging coordination mode in which multiple metal ions are connected to a 2D structure and processes significant interlayer π-π interactions. This result suggests that ligands in combination with tetrazoyl and 2,2'-bipyridyl groups may represent a potential linker for the preparation of new magnetic CPs.

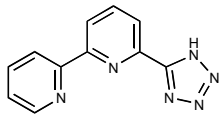

Scheme 1. Molecular structure of Htzbp ligand.

In a continuation of our research, we herein report on the synthesis and characterization of three new coordination polymers, $[M(N_3)(tzbp)]_n$ (M = Cu, **1·Cu**; Mn, **2·Mn**; Co, **3·Co**), by a bifunctional tetrazolate/2,2′-bipyridine ligand**,** 6-(1H-tetrazol-5-yl)-2,2′-bipyridine (Htzbp, Scheme 1), through *in situ*

[2+3] cycloaddition of 6-cayno-2,2′-bipyridine and in the presence of an excess of sodium azide under hydrothermal conditions. With tzbp$^-$ ligands acting in the chelating coordination mode, compound **1·Cu** assumes a single end-on N_3^- (EO-N_3) bridged one-dimensional (1D) zigzag structure. Both compounds **2·Mn** and **3·Co** adopt two-dimensional (2D) layered structures composed of double EO-N_3 bridged dinuclear moieties, [M_2(EO-N_3)$_2$], which are interlinked by tzbp$^-$ ligands in a chelating/bridging mode. The layers of **2·Mn** and **3·Co** are stacked on each in ···ABAB··· and ···AAAA··· fashions, respectively. Magnetic investigations revealed that intrachain antiferromagnetic interactions dominated in compounds **1·Cu**, while **2·Mn** and **3·Co** exhibited spin-canted antiferromagnetism with critical temperatures (T_N) of 3.0 and 18.4 K, respectively. Furthermore, below the T_N, field-induced magnetic transitions of spin-flop and metamagnetism were observed in **2·Mn** and **3·Co**, respectively.

Results and Discussion

Syntheses.

Hydrothermal reactions of 6-cayno-2,2′-bipyridine (bpCN) and different metal salts in the presence of an excess sodium azide resulted in the formation of various coordination polymers with bifunctional a tetrazolate/2,2′-bipyridine ligand (tzbp$^-$). It is noteworthy that the tzbp$^-$ anions in compounds **1·Cu**, **2·Mn** and **3·Co** are generated through [2 + 3] cycloaddition and hydrolysis reactions with the cyano-groups changed to tetrazolate. The IR spectra of **1·Cu**, **2·Mn** and **3·Co** were consistent with the characteristics of their structures. The absence of peaks corresponding to a cyano group in the 2200 cm^{-1} region, indicate that a cyano group is no longer present in the product, and the emergence of a peak at 1400–1500 cm^{-1} indicates the formation of the tetrazole group, consistent with previous reports.[12] Meanwhile, the strong peaks around 2050–2070 cm^{-1} are assigned to the bridging coordination mode of the azide group.

To examine the thermal stabilities of the compounds, thermogravimetric analyses (TGA) were carried out (Supporting Information, Fig. S1). Compounds **1·Cu**, **2·Mn** and **3·Co** were found to be thermally stable without weight loss at temperatures lower than 260°C, 320°C and 300°C, respectively. The structures of **1·Cu**, **2·Mn** and **3·Co** begin to decompose and a rapid weight loss was observed when the temperature reached 280°C, 340 °C and 320 °C, respectively, which can be attributed to the elimination of the tzbp$^-$ and azido groups. X-ray powder diffraction (XRPD) patterns were also carried out for compounds **1·Cu**, **2·Mn** and **3·Co**. The measured XRPD patterns of the three compounds are in good agreement with patterns simulated from the respective single-crystal data for the compounds, thus confirming the bulk purity of the three samples (Figs. S2-S4).

Structure description.

Single crystals of compounds **1·Cu**, **2·Mn** and **3·Co** suitable for single-crystal X-ray crystallography were obtained. Labelled plots of crystal structures are shown in Figs. 1-5 and the selected bond distances and angles are listed in Table S1.

Structure of Compound 1·Cu. Compound **1·Cu** crystallizes in the monoclinic space group $P2_1/c$ and the asymmetric unit contains one crystallographically independent Cu^{2+} ion, one tzbp$^-$ ligand and one azido anion. As shown in Fig. 1, compound **1·Cu** has a covalently bonded zigzag chain structure, in which the Cu^{2+} ions are singly bridged by the EO-N_3 ligands. Each Cu^{2+} ion in **1·Cu** is penta-coordinated with a distorted square pyramidal geometry (τ = 0.27).[13] Three nitrogen atoms (N1–N3) of the tzbp$^-$ ligand and a nitrogen donor (N7) of the azido ligand comprise the basal plane, and the axial coordination sites are occupied by one nitrogen atom (N7A) of the azide group. The bridging EO azido anions are bound asymmetrically to Cu^{2+} with Cu–N distances of 2.048 and 2.880 Å, and the Cu–N_3–Cu angle is 121.26°. The two transoid angles in the basal plane are 156.23° and 160.65°, while the cisoid angles are in the range 73.65°–98.86°. The small bite angles are mainly due to the five-membered ring chelating of tzbp$^-$ ligands. The Cu···Cu distance of 4.314 Å in the chain is rather large compared to that observed in Cu^{2+} compounds with azido anions bridging in an EO mode at the two equatorial positions.[14]

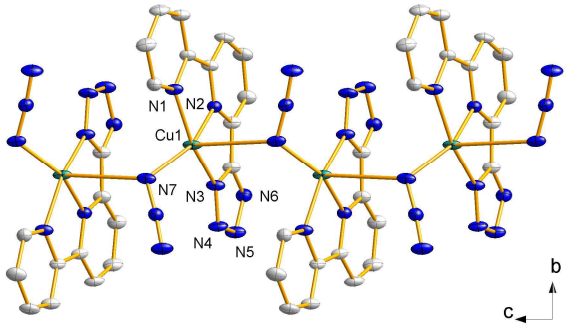

Fig. 1. ORTEP drawing of the uniform chain of **1·Cu** with thermal ellipsoids set at a 50% probability. The H atoms are been omitted for clarity.

Structure of Compound 2·Mn. Single-crystal X-ray diffraction analysis revealed that compound **2·Mn** crystallizes in orthorhombic space groups *P*bca and the asymmetric unit of compound **2·Mn** contains one crystallographically independent Mn^{2+} ion, one tzbp$^-$ ligand and one azido anion. As depicted in Fig. 2, the Mn^{2+} ion displays an distorted octahedral coordination sphere, in which the equatorial positions are occupied by the tridentate NNN atoms from the tzbp$^-$ ligand (N1, N2 and N3) and one nitrogen atom from an azide anion (N7), and the axial positions are occupied by one azido nitrogen (N7A) atom and one tetrazolate nitrogen atom from the tzbp$^-$ ligand (N6B) with Mn–N distances in the range 2.196–2.318 Å. The distortion of the metal polyhedron is mainly due to the small bite angles of the five-membered chelating ring (N1–Mn1–N2, N2–Mn1–N3 and N7–Mn1-N7A at 70.55, 71.79 and 76.73°, respectively). Two neighboring Mn^{2+} ions related by an inversion center are doubly linked by two EO-N_3 bridges (N7 and N7A) resulting a dinuclear [Mn_2(EO-N_3)$_2$] unit, in which the Mn–N–Mn bridging angle and Mn···Mn distance are 103.27° and 3.461 Å, respectively (Fig. 3a). Each Mn_2 unit is further connected to four identical neighboring Mn_2 units by four μ-N^1,N^3-tetrazolate from four tzbp$^-$ ligands and results a 6^3-***hcb*** 2D polymeric layer that is parallel to the *ab* crystal plane (Fig. 3b). The metal coordination spheres of each Mn_2 moiety in the layer display two alternately orientations, in which the dihedral angle of the equatorial planes and the Mn···Mn distance between two tetrazolate-bridged Mn^{2+} ions are

65.89° and 6.444 Å, respectively. Closely related, the dihedral angle of the Mn_2N_2 plane between each Mn_2 moiety is 31.32°. As shown in Fig. 3b, the layers are stacked alternately, so that the Mn_2 units of neighboring 2D layers are directly above the mesh units of another layer (i.e., an ABAB mode). There are some interdigitations between the pyridyl groups that protrude from different sheets through supramolecular π–π stacking (the nearest interlayer Mn···Mn distance is 8.832 Å). The separations between the pyridyl rings of $tzbp^-$ ligands are 3.75 Å for the centroid-centroid distance and 3.34 Å for the interplane distance (Fig. S5).

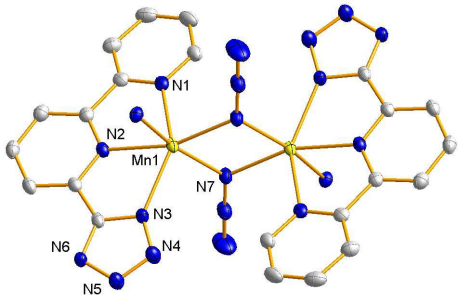

Fig. 2. ORTEP drawing of the local coordination environment of dimeric unit of **2·Mn** with thermal ellipsoids set at a 50% probability. The H atoms are been omitted for clarity.

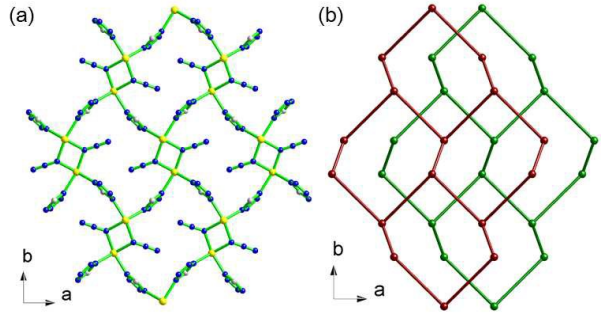

Fig. 3. (a) View of the tetrazole-Mn_2 layer parallel to the *ab* plane in **2·Mn.** (b) The packing of 6^3-***hcb*** net topology of **2·Mn** with Mn ion as the node.

Structure of Compound 3·Co. X-ray analysis reveals that compound **3·Co** crystallizes in the $P2_1/c$ space group and the asymmetric unit contains one crystallographically independent Co^{2+} ion, one $tzbp^-$ ligand and one azido anion. Similar to compound **2·Mn**, compound **3·Co** adopts a 2D layered structure with a $[Co_2(EO\text{-}N_3)_2]$. As shown in Fig. 4, the Co^{2+} center is coordinated in a distorted octahedral sphere occupied by four nitrogen atoms (N1, N2, N3 and N5B) from two $tzbp^-$ ligand and two nitrogen atom (N7 and N7A) from two EO-N_3 group with the Co–N distances in the range 2.086–2.297 Å. The distorted metal polyhedron is mainly due to the small bite angles of the five-membered chelating ring (N1−Co1−N2 and N2−Co1−N3 are 75.39° and 76.45°, respectively). Two neighboring Co^{2+} ions related by an inversion center are linked by two EO-N_3 bridges (N5 and N5A) forming a dinuclear, $[Co_2(EO\text{-}N_3)_2]$, unit. In the unit, the Co–N–Co bridging angle is 101.89° and the Co···Co distance is 3.362 Å. Each Co_2 unit is connected to four neighboring identical Co_2 units through four μ-N^1,N^4-tetrazolate bridges from four $tzbp^-$ ligands, generating a 6^3-***hcb*** layer that is orientated parallel to the *bc* crystal plane (Fig. 5a), where the Co···Co distance spanned by the μ-N^1,N^4-tetrazolate group is 6.370(2) Å. In the layer, the Co_2 moiety shows a systematic alternation of two different orientations, where the dihedral angle of the Co_2N_2 planes is 88.18°. The 3D packing of structure in **3·Co** is unlike that in **2·Mn**, the adjacent layers are packed together in a cavity-above-cavity (···AAAA···) fashion by supramolecular π–π interactions with the nearest interlayer Co···Co distance being 8.25 Å (Fig. 5b). The separations between the pyridyl rings of the $tzbp^-$ ligands are 3.81 Å for the centroid-centroid distance and 3.24 Å for the interplane distance (Fig. S6).

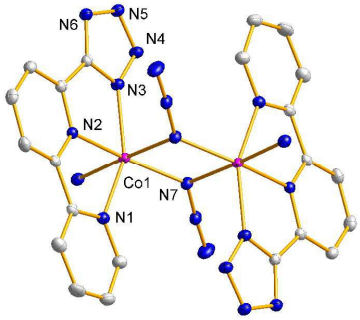

Fig. 4. ORTEP drawing of the local coordination environment of dimeric unit of **3·Co** with thermal ellipsoids set at a 50% probability. The H atoms are been omitted for clarity.

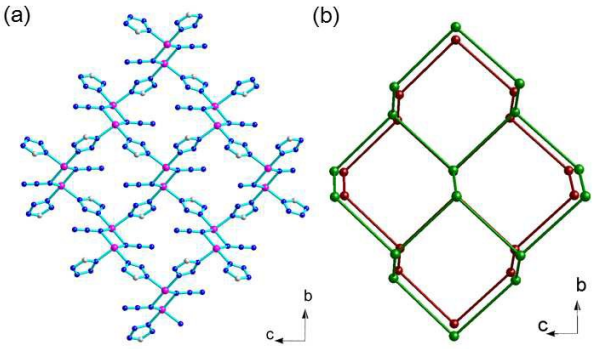

Fig. 5. (a) View of the tetrazole-Mn_2 layer parallel to the *bc* plane in **3·Co.** (b) The packing of 6^3-***hcb*** net topology of **3·Co** with Co ion as the node.

Magnetic Properties.

Compound 1·Cu. The temperature-dependent magnetic susceptibility of a powder sample of **1·Cu** in 2.0–300 K under an applied field of 1.0 kOe is shown in Fig. 6. The $\chi_M T$ value at room temperature is 0.406 $cm^3\ mol^{-1}$ K, slightly larger than the theoretical value of spin-only Cu^{2+} ions (0.375 $cm^3\ mol^{-1}$ K). Upon cooling, the $\chi_M T$ value decreases slightly until 30 K and then rapidly decreases, reaching 0.145 $cm^3\ mol^{-1}$ K at 2.0 K indicating the presence of antiferromagnetic coupling. The magnetic susceptibility above 30 K obeys the Curie−Weiss law very well (Fig. S7), giving a Curie constant C of 0.41 $cm^3\ mol^{-1}$ K and a Weiss constant, θ, of −0.75 K. The negative Weiss constant indicates the existence of antiferromagnetic coupling between the Cu^{2+} ions. For the isotropic Heisenberg antiferromagnetic system with an $S = {}^1/_2$, the molar susceptibility can be expressed as follows based on $H = -JS_iS_{i+1}$:[15]

$$\chi_M = \frac{N\beta^2 g^2}{kT}\frac{0.25+0.14995x+0.30094x^2}{1+1.9862x+0.68854x^2+6.0626x^3} \quad (1)$$

where $x = |J|/kT$. The best fitting for the data from 8 to 300 K gives $J = -0.60$ cm^{-1}, $g = 2.10$ with $R = 3.5 \times 10^{-6}$, and $R = [\sum(\chi_{obsd} - \chi_{calcd})^2/\sum(\chi_{obsd})^2$. The negative J values suggest the existence of antiferromagnetic interactions between the Cu^{2+} ions through the single EO-N_3, which is consistent with literature values, both empirically and theoretically.[16] A magneto-structural correlation based-on several EO-N_3 bridged Cu^{2+} complexes was reported by Thompson et al., in which the magnetic interaction changes from ferromagnetic to antiferromagnetic at Cu−N−Cu angle of 108°.[17] The interaction is found to be ferromagnetic for lower angle values and antiferromagnetic for higher angle values. A reported density functional study for an EO azido-bridged Cu^{2+} binuclear model complex also confirms this empirical conclusion,[18] in which the critical Cu−N−Cu angle was found to be 104°. In the present case, for **1·Cu**, it is clear that the weak antiferromagnetic interaction results from the large Cu−N−Cu angle (121.2°), which is much larger than the critical value of 108°, and the long Cu–N bond distance.

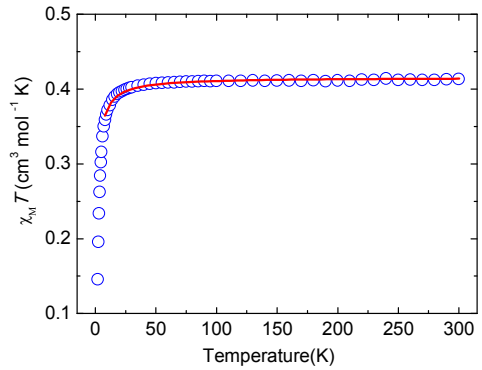

Fig. 6. Plot of $\chi_M T$ vs. T of **1·Cu** in an applied field of 1 kOe from 2 to 300 K. The solid line represents the best fit given in the text.

Compound 2·Mn. The temperature-dependent $\chi_M T$ of **2·Mn** in 2.0–300 K under an applied field of 1.0 kOe is shown in Fig. 7. The $\chi_M T$ value at 300 K is 4.74 cm^3 mol^{-1} K, which is higher than that expected value of 4.38 cm^3 mol^{-1} K for an isolated Mn^{2+} ion ($S = {}^5/_2$ and $g = 2.0$). The $\chi_M T$ value increases gradually upon cooling, reaching a smooth maximum of 5.57 cm^3 mol^{-1} K at 26 K, indicating the ferromagnetic interaction. The χ_M data above 100 K obeys the Curie–Weiss law with a Curie constant $C = 4.56$ cm^3 mol^{-1} K and a Weiss constant $\theta = 10.76$ K (Fig. S8). The positive value of θ confirms that ferromagnetic coupling is dominant. Upon further cooling, the $\chi_M T$ value undergoes an abrupt decrease to 1.08 cm^3 mol^{-1} K at 2.0 K suggesting overall antiferrmagneticism in the low-temperature range. The Néel temperature, as deduced from the peak position of $d\chi_M T/dT$, was $T_N = 3.0$ K. Based on the crystal structure, the magnetic analysis of **2·Mn** was carried out by treating the system as a square lattice of dinuclear units (layer of dimmers). The expression of the magnetic susceptibility for the dimeric moiety (χ_{dimer}) was deduced from an isotropic Heisenberg Hamiltonian: $H = -JS_{Mn1}S_{Mn2}$, where the J is the exchange coupling through the double EO-N_3 bridges. The dimeric units were assumed to have an effective spin associated with the follow equation.

$$S_{eff}(S_{eff}+1) = \frac{2k\chi_{dimer}T}{(Ng^2\beta^2)} \quad (2)$$

The expression [eqn (3)] derived by Curely for a square lattice of classical spins was then used to describe the magnetic properties of the "layer of dimmers" in **2·Mn**.[19]

$$\chi_M = \left[\frac{Ng^2\beta^2 S_{eff}(S_{eff}+1)}{3kT}\right]\left[\frac{(1+u)^2]}{(1-u)^2}\right] \quad (3)$$

where u is the Langevin function, $u = \text{conth}[J_{eff}'S_{eff}(S_{eff}+1)/kT] - kT/[J_{eff}'S_{eff}(S_{eff}+1)]$ with J_{eff}' accounting for the effective magnetic interactions between the Mn_2 units through the μ-N^1,N^3-tetrazolate bridges. The best fit above 10 K leads to $g = 2.02$, $J = 2.09$ cm^{-1}, and $J_{eff}' = -0.23$ cm^{-1}. The obtained values for J and J_{eff}' are in good agreement with those related the Mn^{2+} compounds,[20] and confirm that the magnetic interactions mediated by double EO-N_3 and μ-N^1,N^3-tetrazolate are ferromagnetic and antiferromagnetic, respectively.

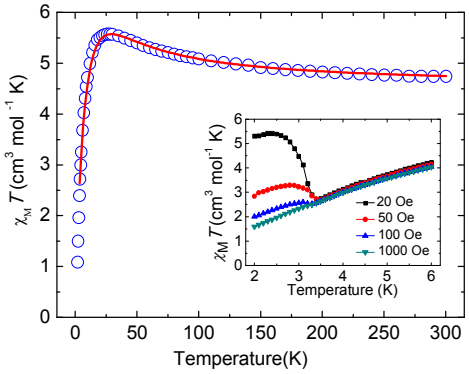

Fig. 7. Plot of $\chi_M T$ vs. T of **2·Mn** in an applied field of 1 kOe from 2 to 300 K. The solid line represents the best fit given in the text. The inset presents the $\chi_M T$ vs T plots at the indicated field.

In addition, the $\chi_M T$ of **2·Mn** becomes field-dependent at low-temperatures (Fig. 7 inset), where $\chi_M T$ abruptly increases below 3.4 K under a weak applied field, suggesting the onset of magnetic ordering due to spin-canted antiferromagnetism and a field-induced magnetic transition.[21] Evidence for magnetic ordering of spin-canted antiferromagnetism was demonstrated by zero-field-cooled/field-cooled (ZFC/FC) magnetization. At 20 Oe, the ZFC/FC shows a divergence below 3.0 K indicating irreversible behavior arising from the formation of a magnetically ordered state (Fig. S9). The presence of magnetic ordering of spin-canted antiferromagnetism was also confirmed by measured alternating current (ac) magnetic susceptibility data, in which a sharp cusp of the in-phase (χ_M') signal at 3.4 K with the corresponding out-of-phase (χ_M'') signals were obtained (Fig. S10).

The isothermal magnetizations $M(H)$ of **2·Mn** were performed at 2.0 K up to 50 kOe (Fig. 8). In the low field region ($H < 10$ kOe), M increases slowly and after a gradual increase, it becomes linear until the field reaches about 40 kOe, where a second change, though a pronounced loss, happens. Such magnetization behavior suggests a spin-flop (SF) magnetic transition.[22] In the SF transition, the antiparallel spin alignment "flops" perpendicular to the applied magnetic field. The H_{SF} and H_C are found at 10.5 and 26.5 kOe, respectively, by dM/dH (Fig. 8,

inset). The M value of 4.14 $N\beta$ at 50 kOe is lower than the expected saturation value of 5.0 $N\beta$ anticipated for a Mn^{2+} ion (S = 5/2, g = 2.0). Furthermore, the magnet-like behavior of **2·Mn** was established by the measurement of a magnetic hysteresis loop, which shows a small hysteresis loop at 2.0 K with a coercive field (H_c) of ~ 80 Oe and a remnant magnetization of 0.0064 $N\beta$ (Fig. 8, inset). The canting angle can be estimated to around 0.07° based on the remnant magnetization.[23]

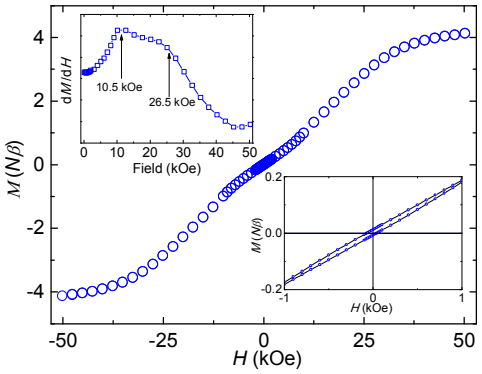

Fig. 8. The isothermal magnetization of **2·Mn** at 2.0 K. The insets give the derivation of M vs H and a blow-up of the hysteresis loop.

To further substantiate the existence of spin-flop, the field dependence of the ac magnetic susceptibilities, $\chi_M'(H)$, at different temperatures and the temperature dependence of FC magnetizations, $\chi_M(T)$, at different fields were collected at different temperatures. As shown in Fig. S11, at 2.0 K, the $\chi_M'(H)$ shows a sharp and a round peak for the transitions of H_{SF} and H_C, respectively, consistent with the dM/dH results. This two transitions in $\chi_M'(H)$ become weakened and disappear as the temperatures increase. Fig. S12 represents the $\chi_M(T)$ at different applied fields. Under an applied field of 1 kOe, the χ_M versus T curve initially increases with decreasing temperature, reaching a sharp maximum, and then drops rapidly to 2 K. However, the FC curves at 9 kOe and above show no maximum, indicating the spins under a larger field (>10 kOe) flop to the direction perpendicular to the field. Both behaviors are important features of the spin-flop characteristics. Combing $\chi_M(T)$ and $\chi_M'(H)$ data, the magnetic phase (T, H) diagram of **2·Mn** was constructed and is shown in the Fig. S13. On an analysis of the M–H curves, the solid H_{SF} (T) and H_C (T) lines in the Fig. S13, signify the transitions from AF to SF and SF to P, respectively, corresponding to spin-flop materials.

General speaking, spin canting can arise from two contributions: (1) the presence of an antisymmetric exchange (Dzyaloshinsky−Moriya interaction) and (2) existence of single-ion magnetic anisotropy.[24] The presence of an inversion center between adjacent spin centers can result in the disappearance of the antisymmetric exchange. Hence, the lack of antisymmetric exchange in compound **2·Mn** would be expected, due to the existence of an inversion center between the Mn^{2+} ions. However, the Mn1 center in **2·Mn** displays a highly distorted octahedral geometry, which were reported as originating from the weak single-ion anisotropy of the high-spin Mn^{2+} site.[22,25] Therefore, we assume that the spin-canted antiferromagnetism in **2·Mn** can be attributed to weak single-ion magnetic anisotropy of distorted Mn^{2+} site.

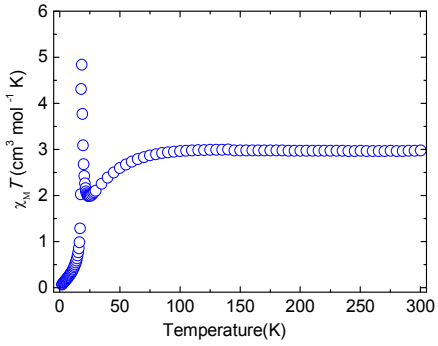

Fig. 9. Plot of $\chi_M T$ vs. T of **3·Co** in an applied field of 1 kOe from 2 to 300 K.

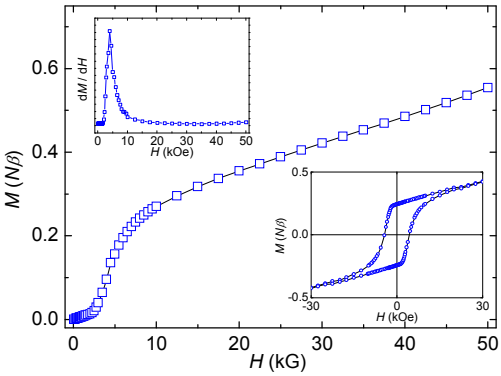

Fig. 10. Field dependence of the magnetization of **3·Co** at 2.0 K. The insets give the derivation of M vs H and a blow-up of the hysteresis loop.

Compound 3·Co. The $\chi_M T$ vs. T for compound **3·Co** is shown in Fig. 9. At 300 K, the $\chi_M T$ value is 3.46 $cm^3\ mol^{-1}$ K, which is greater than the excepted value for a high-spin Co^{2+} ion (1.87 $cm^3\ mol^{-1}$ K with g = 2.0). Upon cooling, the $\chi_M T$ first decreases smoothly, reaching a minimum value of 2.03 $cm^3\ mol^{-1}$ K at 25 K, then rises rapidly, reaching a sharp maximum value of 5.14 $cm^3\ mol^{-1}$ K at 18.5 K and finally drops again to 0.08 $cm^3\ mol^{-1}$ K at 2.0 K. The data above 50 K obeys the Curie–Weiss law with a Curie constant C = 3.01 $cm^3\ mol^{-1}$ K and a Weiss constant θ = −2.67 K (Fig. S14). The continuous decrease in $\chi_M T$ from 300 K to 25 K can be attributed to both the spin-orbit coupling of the octahedral Co^{2+} ions and the moderate antiferromagnetic coupling in **3·Co**. The abrupt increase in $\chi_M T$ at temperatures below 25 K suggests spin-canted antiferromagnetism, while the final rapid drop in $\chi_M T$ at temperatures below 18.5 K may be due to interlayer antiferromagnetic ordering and/or saturation effects. The ZFC/FC magnetizations of **3·Co** performed at 100 Oe (Fig. S15) were non-bifurcated and show a sharp maximum at 18.4 K suggesting the occurrence of antiferromagnetic ordering with T_N = 18.4 K. The temperature dependence of the ac susceptibility of **3·Co** was also measured at a zero dc field (Fig. S16), which shows a sharp frequency-independent of χ_M' signals with the absence of χ_M'' signals, thus confirming the onset of antiferromagnetic ordering and implies the existence of a magnetic phase transition.

The field dependence of the magnetizations of **3·Co** at 2.0 K (Fig. 10) shows a sigmoidal shape with an abrupt increase at a field above 2.8 kOe to reach a value of 0.42 Nβ at 50 kOe. This

sigmoidal magnetization clearly indicates a field-induced magnetic transition of metamagnetism.[21] In the metamagnetic transition, the net moments aligned antiparallel by weak antiferromagnetic interactions are overcome by an external field, resulting in the state going from AF to P. The critical field of transition, H_C, at 2.0 K was estimated to be about 3.6 kOe determined by dM/dH. The M value of 0.42 $N\beta$ at 50 kOe is far below the expected saturation value of 2−3 $N\beta$ for an isotropic high-spin Co^{2+} system, confirming the antiferromagnetic nature of **3·Co**. In addition, a hysteresis loop is clearly obvious at 2.0 K, (Fig. 10, inset), indicating hard magnet behavior. The hysteresis loop shows a remnant magnetization of 0.24 $N\beta$ and a coercive field of 3.8 kOe. Based on the remnant magnetization at 2.0 K, the canting angle is estimated to be approximately 6.4°.[23]

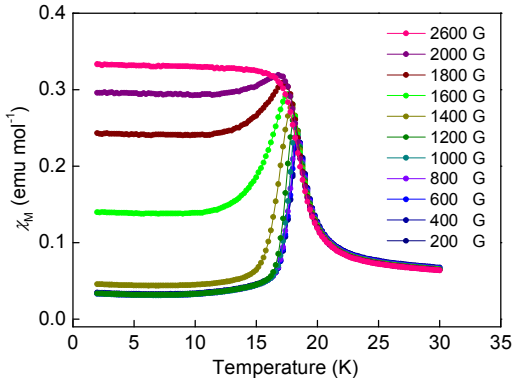

Fig. 11. FC magnetization curves measured under different external fields for compound **3·Co**.

The magnetic phase transition for compound **3·Co** was further investigated by the measurements of various fields of the FC magnetic susceptibilities, $\chi_M(T)$, and the field dependence of the magnetizations, $M(H)$, at different temperatures. As shown in Fig. 11, the maximum of $\chi_M(T)$ shifts to lower temperature with increasing applied field, until the $\chi_M(T)$ reaches a plateau at a field larger than 2000 Oe, indicating that the weak interlayer antiferromagnetic interaction is overcome by the external field. As shown in Fig. S17, at 2.0 K, the step-wise $M(H)$ curve clearly indicates field-induced magnetic transition from AF to P. This step-wise magnetization becomes less pronounced with increasing temperature, and the differentials of these curves show peaks that shift to lower fields with increasing temperature (Fig. S18) indicating the phase transitions of metamagnetism. Combining $M(H)$, FCM and the frequency-independent χ_M' data, the magnetic phase (T, H) diagram was plotted in Fig. S19. The H_C decreases with increasing temperature and finally disappears at about 18.4 K. The solid line of H_C (T) in Fig. S19, on an analysis of the M–H curves, signifies a typical magnetic transition from AF to P corresponding to metamagnetic materials.

Taking into account the structural features of compound **3·Co**, although the adjacent spin Co^{2+} ions are related to a crystallographic inversion center, all of the $[Co_2(EO\text{-}N_3)_2]$ moieties are connected by 2_1 helices with opposite chirality. The different orientations of opposite chirality may induce the occurrence of antisymmetric exchange, thus resulting in spin canting. Moreover, the highly distorted octahedral Co^{2+} site might exhibit considerable anisotropy, which also provides a contribution to the spin canting in **3·Co**. Similar results have been observed in several compounds with same space group.[26]

The structural and magnetic properties of compounds **1·Cu-3·Co** are comparable to those of known compounds with similar structures and dimensionalities. For compound **1·Cu**, the Cu^{2+} ions are linked by single EO-N_3 to form a 1D chain and the overall AF exchange interactions are observed with no long-range ordering above 2.0 K, which is consist with the results for 1D Cu^{2+} compound with single EO-N_3 bridging.[27] The 2D layered structure of **2·Mn** and **3·Co** is similar to those of reported 2D compound composing a $[M_2(EO\text{-}N_3)_2]$ building unit.[28] Compound **2·Mn** crystallizes in centrosymmetric space group *P*bca, which forbid the occurrence of antisymmetric interaction due to the presence of inversion centers between the Mn^{2+} sites. Thus, the spin canting in **2·Mn** can be attracted by single-ion magnetic anisotropy. In contrast, although the adjacent spin Co^{2+} ions in compound **3·Co** are related to a crystallographic inversion center, all of the $[Co_2(EO\text{-}N_3)_2]$ units are linked by 2_1 helices with opposite chirality. Thus, the spin canting **3·Co** was attracted by both of antisymmetric interaction and single-ion magnetic anisotropy.

Conclusions

The introduction of a bifunctional ligand, Htzbp, in combination with tetrazoyl and 2,2'-bipyridyl groups, permitted three new azide-based coordination polymers to be synthesized. With $tzbp^-$ ligands functioning as a chelating coordination mode, compound **1·Cu** adopts a single end-on N_3^- (EO-N_3) bridged 1D zigzag structure, while **2·Mn** and **3·Co** adopts 2D layered structures comprised of double EO-N_3 bridged dinuclear motifs, $[M_2(EO\text{-}N_3)_2]$, interlinked by chelating/bridging of $tzbp^-$ ligands. Magnetic studies reveal the existence of intrachain antiferromagnetic interactions that are dominant in compound **1·Cu**. Compounds **2·Mn** and **3·Co** exhibit spin-canted antiferromagnetism with T_N = 3.0 and 18.4 K, respectively. In addition, below T_N, the field-induced magnetic transitions of spin-flop and metamagnetism for **2·Mn** and **3·Co,** respectively, were also observed. The studies show that the use of bifunctional tetrazolate/2,2′-bipyridine ligand is particularly promising for use in the construction of extended networks containing a highly distorted metal site that can give rise to versatile bulk magnetic behavior.

Experimental Section

Synthesis

All solvents and reagents where used as received, no purification was necessary. All reactions were performed under aerobic conditions. *Caution!* Azido compounds are potentially explosive; such compounds should be synthesized and used in small quantities and treated with the utmost care at all times. The precursor of 6-cayno-2,2′-bipyridine was prepared as previously reported.[29]

$[Cu(N_3)(tzbp)]_n$ (1·Cu). A mixture of $Cu(ClO_4)_2{\cdot}6H_2O$ (23 mg, 0.062 mmol), 6,6′-dicayno-2,2′-bipyridine (bpCN, 23 mg, 0.125 mmol), NaN_3 (17 mg, 0.25 mmol), DMF (6ml) and H_2O (1 mL) was placed in a Teflon reactor (25 mL) and heated at 100 °C for two days. After the mixture was gradually cooled to room

temperature at a rate of 1 °C h^{-1}, dark-green crystals of **1·Cu** suitable for X-ray study were obtained. The solid product was washed with water, isolated by suction filtration and dried in air. Yield: 43% (based on bpCN). A powder X-ray diffraction pattern of the bulk sample compared well with the pattern simulated from the single-crystal data (vide infra). Anal. Calcd (found) for $C_{11}H_7CuN_9$: C, 40.45; H, 2.02; N, 38.27. Found: C, 40.14; H, 2.13; N, 38.32. IR data (KBr disk, cm^{-1}): 2072(s), 2051(vs), 1615 (m), 1602 (m), 1575 (m), 1489 (m), 1458 (s), 1442 (s), 1378 (w), 1332 (w), 1257 (w), 1177 (m), 1147 (m), 1037 (w), 1012 (m), 827 (w), 799 (s), 787 (s), 762 (m), 730 (m) , 696 (m), 662 (m), 603 (w).

$[Mn_2(N_3)_2(tzbp)]_n$ (2·Mn). A mixture of $Mn(ClO_4)_2·6H_2O$ (90.1 mg, 0.25 mmol), 6-cayno-2,2′-bipyridine (bpCN, 46 mg, 0.25 mmol), and NaN_3 (50 mg, 0.75 mmol) in H_2O (6 mL) was placed in a Teflon reactor (25 mL). The mixture was heated according to the following temperature program: increasing the temperature to 160 °C at 18.3 °C/h, holding at 160 °C for 72 h, and then cooling to 30 °C at a rate of 2.3 °C/h. The yellow block crystals of **2·Mn** suitable for single-crystal X-ray diffraction analysis were obtained. The crystals were rinsed a few times with H_2O and dried in air. Yield: 47% (based on bpCN). A powder X-ray diffraction pattern of the bulk sample compared well with the pattern simulated from the single-crystal data (vide infra). Anal. Calcd for $C_{11}H_7MnN_9$: C, 41.56; H, 2.41; N, 38.98. Found: C, 41.26; H, 2.19; N, 39.39. IR data (KBr disk, cm^{-1}): 2055 (vs), 1610 (s), 1594 (s), 1574 (s), 1479 (w), 1433 (s), 1373 (m), 1323 (s), 1276 (w), 1016 (w), 1005 (w), 1153 (m), 790 (s), 759 (s), 741 (s), 691 (s) , 651 (m), 607 (w).

$[Co_2(N_3)_2(tzbp)]_n$ (3·Co). A solution of $Co(ClO_4)_2·6H_2O$ (91.1 mg, 0.25 mmol), 6-cayno-2,2′-bipyridine (bpCN, 45 mg, 0.25 mmol), and NaN_3 (50 mg, 0.75 mmol) in H_2O (6 mL) was placed in a Teflon reactor (25 mL). The mixture was heated according to the following temperature program: increasing the temperature to 140 °C at 18.3 °C/h, holding at 140 °C for 72 h, and then cooling to 30 °C at a rate of 2.3 °C/h. The orange block crystals suitable for single-crystal X-ray diffraction analysis were obtained. The crystals were rinsed a few times with H_2O and dried in air. Yield: 52 % (based on bpCN). A powder X-ray diffraction pattern of the bulk sample compared well with the pattern simulated from the single-crystal data (vide infra). Anal. Calcd for $C_{11}H_7CoN_9$: C, 40.72; H, 2.16; N, 38.87. Found: C, 41.17; H, 2.55; N, 38.95. IR data (KBr disk, cm^{-1}): 2066 (vs), 1600 (s), 1574 (m), 1556 (m), 1532 (s), 1515 (w), 1482 (w), 1467 (s), 1463 (m), 1440 (s), 1402 (w), 1369 (w), 1178 (m), 1153 (m), 1023 (w), 1009 (w), 829 (w), 785 (s), 762 (s), 737 (s), 690 (s) , 655 (m), 634 (m), 602 (w).

Crystallographic Measurements

The single crystals of compounds **1·Cu**, **2·Mn** and **3·Co** were mounted on the tip of a glass fiber with dimensions of 0.19 × 0.14 × 0.05 mm, 0.26 × 0.20 × 0.11 mm, and 0.19 × 0.18 × 0.15 mm, respectively. Intensity data were collected at 150 (2) K within the limits of 2.43° < θ < 30.01° for **1·Cu**, 2.75° < θ < 30.48° for **2·Mn**, and 2.62° < θ < 28.28° for **3·Co** using a Brucker-Nonius APEXII CCD diffractometers with graphite-monochromated Mo Kα radiation (λ = 0.7107 Å). The structures were solved by conventional methods and refined by full-matrix least-squares on all F2 data using SHELX2014 in conjunction with the Olex2[30] graphical user interface. All non-hydrogen atoms were refined anisotropically, whereas the hydrogen atoms were placed in ideal, calculated positions, with isotropic thermal parameters riding on their respective carbon atoms. Experimental details for X-ray data collection and the refinements of compounds **1·Cu**, **2·Mn** and **3·Co** are presented in Table 1.

Magnetic measurement

Variable temperature dc magnetic susceptibility measurements and ac magnetic susceptibility measurements were collected on microcrystalline samples, restrained in eicosane to prevent torquing, on a Quantum Design MPMS-7 SQUID and a PPMS magnetometer equipped with 7.0 T and 9.0 T magnets, respectively, operated in the range of 2.0–300.0 K. Diamagnetic corrections were estimated from Pascal's constants[31] and subtracted from the experimental susceptibility data to obtain the molar paramagnetic susceptibility of the compounds.

Other Studies

Infrared spectra were recorded for the solid state (KBr pellets) on a Nicolet Magna 550 FTIR spectrometer in the range of 4000-400 cm^{-1}. Elemental analyses were carried out using an Elementar Vario EL III analyzer. Thermogravimetric analysis was performed on a Seiko Instrumental, Inc., EXSTAR6000 TG/DTA 6200 analyzer with a heating rate of 5 °C/min under a nitrogen atmosphere. Powder diffraction data were recorded on a SHIMADZU XRD-6000 X-ray diffractometer at 30 kV and 30 mA with Cu-Kα radiation (λ = 1.5406 Å), with a step size of 0.028 in θ and a scan speed of 1 s per step.

Acknowledgment

The authors gratefully acknowledge financial support for this work from the Tunghai University, and the Ministry of Science and Technology of Taiwan (MOST 104-2113-M-029-006). We also thank instrumental supporting and measuring by Prof. Hui-Lien Tsai and Dr. Min Kai Lee at National Cheng Kung University.

Notes and references

Department of Chemistry, Tunghai University, Taichung 407, Taiwan. Fax: 886 -4-23590426; E-mail: ciyang@thu.edu.tw

† Electronic Supplementary Information (ESI) available: Detailed experimental procedures, TGA plots, PXRD patterns, additional crystallographic diagrams and other magnetic diagram. CCDC 1439545-1439547. For ESI and crystallographic data in cif or other electronic format. See DOI: 10.1039/b000000x/

1 (a) R. D. Willet, D. Gatteschi and O. Kahn, *Magneto-Structural Correlations in Exchange Coupled Systems*, Reidel Publishing, Dordrecht, 1985; (b) O. M. Yaghi, M. O'Keeffe, N. W. Ockwig, H. K. Chae, M. Eddaoudi and J. Kim, *Nature*, 2003, **423**, 705; (c) E. Coronado and G. Minguez Espallargas, *Chem. Soc. Rev.*, 2013, **42**, 1525; (d) S. Chaemchuen, N. A. Kabir, K. Zhou and F. Verpoort, *Chem. Soc. Rev.*, 2013, **42**, 9304.

2 (a) N. Roques**,** V. Mugnainin and J. Veciana**,** *Top. Curr. Chem.***,** 2010**, 293,** 207; (b) Y.-G. Huang, F.-L. Jiang and M.-C. Hong, *Coord. Chem. Rev.*, 2009, **253**, 2814; (c) M. Kurmoo, *Chem. Soc. Rev*., 2009, **38**, 1353; (d) Y.-F. Zeng, X. Hu, F.-C. Liu and X.-H. Bu, *Chem. Soc. Rev*., 2009, **38**, 469; (e) D. Gatteschi, O. Kahn, J. S. Miller and F. Palacio, *Magnetic Molecular Materials*, Kluwer

Academic, Dordrecht, The Netherlands, 1991; (f) O. M. Yaghi, G. Li and H. Li, *Nature*, 1995, **378**, 703; (g) K. Maruoka, N. Murase and H. Yamamoto, *J. Org. Chem.*, 1993, **58**, 2938; (h) C.-T. Chen and K. S. Suslick, *Coord. Chem. Rev*., 1993, **128**, 293.

3 J. V. Barth, G. Costantini and K. Kern, *Nature*, 2005, **437**, 671; (b) M. Murrie, S. Parsons and R. E. P. Winpenny, *J. Chem. Soc., Dalton Trans.*, 1998, 1423; (a) J. V. Barth, G. Costantini and K. Kern, *Nature*, 2005, **437**, 671; (b) M. Murrie, S. Parsons and R. E. P. Winpenny, *J. Chem. Soc., Dalton Trans.*, 1998, 1423; (c) A. Saitoh, H. Miyasaka, M. Yamashita and R. Clérac, *J. Mater. Chem.*, 2007, **17**, 2002; (d) D. J. Collins and H.-C. Zhou, *J. Mater. Chem.*, 2007, **17**, 3154; (e) B. Moulton and M. J. Zaworotko, *Chem. Rev.*, 2001, **101**, 1629; (f) W. Su, M. Hong, J. Weng, R. Cao and S. Lu, *Angew. Chem.*, 2000, **39**, 2911; (g) P. J. Hagrman, D. Hagrman and J. Zubieta, *Angew. Chem. Int. Ed.*, 1999, **38**, 2638; (h) A. Guijarro, O. Castillo, L. Welte, A. Calzolari, P. J. S. Miguel, C. J. Gómez-García, D. Olea, R. di Felice, J. Gómez-Herrero and F. Zamora, *Adv. Funct. Mater.*, 2010, **20**, 1451.

4 (a) L. M. Toma, C. Ruiz-Pérez, J. Pasán, W. Wernsdorfer, F. Lloret and M. Julve, *J. Am. Chem. Soc.*, 2012, **134**, 15265; (b) A. V. Palii, O. S. Reu, S. M. Ostrovsky, S. I. Klokishner, B. S. Tsukerblat, Z.-M. Sun, J.-G. Mao, A. V. Prosvirin, H.-H. Zhao and K. R. Dunbar, *J. Am. Chem. Soc.*, 2008, **130**, 14729; (c) E. Coronado, J. R. Galán-Mascarós and C. Martí-Gastaldo, *J J. Am. Chem. Soc.*, 2008, **130**, 14987; (d) K. C. Mondal, G. E. Kostakis, Y. Lan, C. E. Anson and A. K. Powell, *Inorg. Chem.*, 2009, **48**, 9205; (e) S. O. Gutschke, D. J. Price, A. K. Powell and P. T. Wood, *Angew. Chem. Int. Ed.*, 1999, **38**, 1088; (f) H. Miyasaka, *Acc. Chem. Res.*, 2013, **46**, 248.

5 (a) J. Ribas, A. Escuer, M. Monfort, R. Vicente, R. Cortés, L. Lezama and T. Rojo, *Coord. Chem. Rev.*, 1999, **193–195**, 1027; (b) X.-Y. Wang, Z.-M. Wang and S. Gao, *Chem Commun.*, 2008, 281; (c) Z. He, Z.-M. Wang, S. Gao and C.-H. Yan, *Inorg. Chem.*, 2006, **45**, 6694; (d) R.-Y. Li, X.-Y. Wang, T. Liu, H.-B. Xu, F. Zhao, Z.-M. Wang and S. Gao, *Inorg. Chem.*, 2008, **47**, 8134; (e) J.-Y. Zhang, K. Wang, X.-B. Li and E.-Q. Gao, *Inorg. Chem.*, 2014, **53**, 9306; (f) P. Kar, M. G. B. Drew, C. J. Gómez-García and A. Ghosh, *Inorg. Chem.*, 2013, **52**, 1640.

6 (a) X.-Y. Wang, H.-Y. Wei, Z.-M. Wang, Z.-D. Chen and S. Gao, *Inorg. Chem.*, 2005, **44**, 572; (b) T. Wen, M. Li, X.-P. Zhou and D. Li, *Dalton Trans.*, 2011, **40**, 5684; (c) P. Manna, B. K. Tripuramallu, S. Bommakanti and S. K. Das, *Dalton Trans.*, 2015, **44**, 2852; (d) X.-Y. Wang, Z.-M. Wang and S. Gao, *Chem Commun.*, 2007, 1127; (e) R. A. Agarwal, A. Aijaz, M. Ahmad, E. C. Sañudo, Q. Xu and P. K. Bharadwaj, *Cryst. Growth Des.*, 2012, **12**, 2999.

7 (a) K. Liu, W. Shi and P. Cheng, *Dalton Trans.*, 2011, **40**, 8475; (b) L. Yi, B. Ding, B. Zhao, P. Cheng, D.-Z. Liao, S.-P. Yan and Z.-H. Jiang, *Inorg. Chem.*, 2004, **43**, 33; (c) J. P. Zhang, S. L. Zheng, X. C. Huang and X. M. Chen, *Angew. Chem.*, 2004, **116**, 208; (d) Q. Ye, Y.-H. Li, Y.-M. Song, X.-F. Huang, R.-G. Xiong and Z. Xue, *Inorg. Chem.*, 2005, **44**, 3618; (e) D. Li, T. Wu, X. P. Zhou, R. Zhou and X. C. Huang, *Angew. Chem. Int. Ed.*, 2005, **44**, 4175; (f) H. Park, D. M. Moureau and J. B. Parise, *Chem. Mater.*, 2006, **18**, 525; (g) M. Wriedt, A. A. Yakovenko, G. J. Halder, A. V. Prosvirin, K. R. Dunbar and H.-C. Zhou, *J. Am. Chem. Soc.*, 2013, **135**, 4040; (h) Z. Yan, M. Li, H.-L. Gao, X.-C. Huang and D. Li, *Chem Commun.*, 2012, **48**, 3960.

8 (a) A.-X. Zhu, J.-B. Lin, J.-P. Zhang and X.-M. Chen, *Inorg. Chem.*, 2009, **48**, 3882; (b) T. Yang, H. Cui, C. Zhang, L. Zhang and C.-Y. Su, *Inorg. Chem.*, 2013, **52**, 9053; (c) R.-B. Lin, D. Chen, Y.-Y. Lin, J.-P. Zhang and X.-M. Chen, *Inorg. Chem.*, 2012, **51**, 9950; (d) Z. Yan, M. Li, H.-L. Gao, X.-C. Huang and D. Li, *Chem. Commun.*, 2012, **48**, 3960; (e) W.-Y. Gao, W. Yan, R. Cai, K. Williams, A. Salas, L. Wojtas, X. Shi and S. Ma, *Chem. Commun.*, 2012, **48**, 8898; (f) W.-Y. Gao, R. Cai, L. Meng, L. Wojtas, W. Zhou, T. Yildirim, X. Shi and S. Ma, *Chem. Commun.*, 2013, **49**, 10516; (g) M. Wriedt, A. A. Yakovenko, G. J. Halder, A. V. Prosvirin, K. R. Dunbar and H.-C. Zhou, *J. Am. Chem. Soc.*, 2013, **135**, 4040.

9 (a) D. Gatteschi, O. Kahn, J. S. Miller and F. Palacio, *Magnetic Molecular Materials*, Kluwer Academic, Dordrecht, 1991; (b) . S. Miller, *Adv. Mater.* 2002, **14**, 1105; (c) W. Zhang, F. Zhao, T. Liu, M. Yuan, Z. M. Wang and S. Gao, *Inorg. Chem.*, 2007, **46**, 2541; (d) Y. F. Yue, J. Liang, E. Q. Gao, C. J. Fang, Z. G. Yan and C. H. Yan, *Inorg. Chem.*, 2008, **47**, 6115; (e) X. Y. Wang, Z. M. Wang and S. Gao, *Inorg. Chem.*, 2008, **47**, 5720; (f) Z. Weng, Z. Chen and F. Liang, *Inorg. Chem.*, 2009, **48**, 8703; (g) D. Sarma, P. Mahata, S. Natarajan, P. Panissod, G. Rogez and M. Drillon, *Inorg. Chem.*, 2012, **51**, 4495; (h) W. Ouellette, J. R. Galan-Mascaros, K. R. Dunbar and J. Zubieta, *Inorg. Chem.*, 2006, **45**, 1909.

10 (a) X. Wang, J. Peng, M.-G. Liu, D.-D. Wang, C.-L. Meng, Y. Li and Z.-Y. Shi, *CrystEngComm*, 2012, **14**, 3220; (b) B.-Y. Wu, C.-I Yang, M. Nakano and G.-H. Lee, *Dalton Trans*., 2014, **43**, 47; (c) K. Darling, W. Ouellette, A. Prosvirin, S. Freund, K. R. Dunbar and J. Zubieta, *Cryst. Growth Des.*, 2012, **12**, 2662; (d) W. Ouellette and J. Zubieta, *Chem. Commun.*, 2009, 4533; (e) O. Sengupta and P. S. Mukherjee, *Inorg. Chem.*, 2010, **49**, 8583; (f) X.-B. Li, G.-M. Zhuang, X. Wang, K. Wang and E.-Q. Gao, *Chem. Commun.*, 2013, **49**, 1814-1816; (g) A. Thibon, J. F. Bartoli, S. Bourcier and F. Banse, *Dalton Trans.*, 2009, 9587.

11 J.-D. Tsai, C.-I. Yang, *Dalton Trans.*, 2014, **43**, 15576.

12 (a) J. Tao, Z. J. Ma, R. B. Huang and L. S. Zheng, *Inorg. Chem.*, 2004, **43**, 6133; (b) W. C. Song, J. R. Li, P. C. Song, Y. Tao, Q. Yu, X. L. Tong and X. H. Bu, *Inorg. Chem.*, 2009, **48**, 3792; (c) T.-W. Tseng, T.-T. Luo, S.-Y. Chen, C.-C. Su, K.-M. Chi and K.-L. Lu, *Cryst. Growth Des.*, 2013, **13**, 510.

13 A. W. Addison, T. N. Rao, J. Reedijk, J. V. Rijn, G. C. Verschoor, *J. Chem. Soc., Dalton Trans.*, 1984, 1349.

14 (a) G.-F. Liu, Z.-G. Ren, H.-X. Li, Y. Chen, Q.-H. Li, Y. Zhang and J.-P. Lang, *Eur. J. Inorg. Chem.*, 2007, 5511; (b) T. C. Stamatatos, G. S. Papaefstathiou, L. R. MacGillivray, A. Escuer, R. Vicente, E. Ruiz and S. P. Perlepes, *Inorg. Chem.*, 2007, **46**, 8843; (c) Z.-G. Gu, J.-L. Zuo and X.-Z. You, *Dalton Trans.*, 2007, 4067; (d) Y. Z. Zhang, H. Y. Wei, F. Pan, Z. M. Wang, Z. D. Chen and S. Gao, *Angew. Chem., Int. Ed.*, **117**, 5991; (e) P. S. Mukherjee, T. K. Maji, G. Mostafa, T. Mallah and N. R. Chaudhuri, *Inorg. Chem.*, 2000, **39**, 5147.

15 W. E. Estes, D. P. Gavel, W. E. Hatfield and D. J. Hodgson, *Inorg. Chem.*, 1978, **17**, 1415.

16 A. Escuer, R. Vicente, F. A. Mautner and M. A. S. Goher, *Inorg. Chem.*, 1997, **36**, 1233.

17 S. S. Tandon, L. K. Thompson, M. E. Manuel and J. N. Bridson, *Inorg. Chem.*, 1994, **33**, 5555.

18 E. Ruiz, J. Cano, S. Alvarez and P. Alemany, *J. Am. Chem. Soc.*, 1998, **120**, 11122.

19 (a) A. Rodríguez-Diéguez, J. Cano, R. Kivekäs, A. Debdoubi and E. Colacio, *Inorg. Chem.*, 2007, **46**, 2503; (b) Y.-Q. Tian, C.-X. Cai, X.-M. Ren, C.-Y. Duan, Y. Xu, S. Gao and X.-Z. You, *Chem.–Eur. J.*, 2003, **9**, 5673.

20 (a) M.-M. Yu, Z.-H. Ni, C.-C. Zhao, A.-L. Cui and H.-Z. Kou, *Eur. J. Inorg. Chem.*, 2007, **2007**, 5670; (b) A. Escuer, B. Cordero, M. Font-Bardia, T. Calvet, O. Roubeau, S. J. Teat, S. Fedi and F. Fabrizi de Biani, *Dalton Trans.*, 2010, **39**, 4817; (c) S.-Q. Bai, E.-Q. Gao, Z. He, C.-J. Fang, Y.-F. Yue and C.-H. Yan, *Eur. J. Inorg. Chem.*, 2006, **2006**, 407.

21 (a) W.-K. Chang, R.-K. Chiang, Y.-C. Jiang, S.-L. Wang, S.-F. Lee and K.-H. Lii, *Inorg. Chem.*, 2004, **43**, 2564; (b) X. Hao, Y.-G. Wei and S.-W. Zhang, *Chem. Commun*., 2000, 2271; (c) H.-Z. Kou, S. Gao, W.-M. Bu, D.-Z. Liao, B.-Q. Ma, Z.-H. Jiang, S.-P. Yan, Y.-G. Fan and G.-L. Wang, *Dalton Trans.*, 1999, 2477; (d) H.-Z. Kou, W.-M. Bu, S. Gao, D.-Z. Liao, Z.-H. Jiang, S.-P. Yan, Y.-G. Fan and G.-L. Wang, *Dalton Trans.*, 2000, 2996.

22 (a) R. L. Carlin and A. J. Van Duyneveldt, *Acc. Chem. Res.*, 1980, **13**, 231; (b) J. L. Manson, C. R. Kmety, F. Palacio, A. J. Epstein and J. S. Miller, *Chem. Mater.*, 2001, **13**, 1068; (c) D. Pinkowicz, M. Rams, W. Nitek, B. Czarnecki and B. Sieklucka, *Chem. Commun.*, 2012, **48**, 8323; (d) Y.-B. Lu, M.-S. Wang, W.-W. Zhou, G. Xu, G.-C. Guo and J.-S. Huang, *Inorg. Chem.*, 2008, **47**, 8935.

23 (a) J.-R. Li, Q. Yu, E. C. Sanudo, Y. Tao and X.-H. Bu, *Chem. Commun.*, 2007, 2602; (b) F. Palacio, M. Andrés, R. Horne and A. J. van Duyneveldt, *J. Magn. Magn. Mater.*, 1986, **54**, 1487.

24 (a) A. Rodriguez-Dieguez, M. A. Palacios, A. Sironi and E. Colacio, *Dalton Trans.*, 2008, 2887; (b) N. Liu, Q. Yue, Y.-Q. Wang, A.-L.

Cheng and E.-Q. Gao, *Dalton Trans.*, 2008, 4621; (c) A. Rodriguez, R. Kivekas and E. Colacio, *Chem. Commun.*, 2005, 5228.

25 (a) J. A. Schlueter, J. L. Manson, K. A. Hyzer and U. Geiser, *Inorg. Chem.*, 2004, **43**, 4100; (b) X.-Y. Wang, L. Wang, Z.-M. Wang, G. Su and S. Gao, *Chem. Mater.*, 2005, **17**, 6369; (c) R. L. Carlin, in *Magnetochemistry*, Springer, 1986, pp. 237.

26 (a) R. L. Carlin and A. J. V. Duyneveldt, *Magnetic Properties of Transition Metal Compounds*, Springer, New York, 1977; (b) A. Bellitto, F. Federici, M. Colapietro, G. Portalone and D. Caschera, *Inorg. Chem.* 2002, **41**, 709; (c) B. Liu, R. Shang, K.-L. Hu, Z.-M. Wang and S. Gao, *Inorg. Chem.*, 2012, **51**, 13363; (d) X.-N. Cheng , W. Xue , W.-X. Zhang and X.-M. Chen, *Chem. Mater.*, 2008, **20**, 5345; (e) J. Huang, G. Wu, J. Bai, Y. Jiang, G. Li, S. Qiu and R. Clerac, *Inorg. Chem.*, 2013, **52**, 11051; (f) T. T. Wang, M. Ren, S. S. Bao, B. Liu, L. Pi, Z. S. Cai, Z. H. Zheng, Z. L. Xu and L. M. Zheng, *Inorg. Chem.*, 2014, **53**, 3117; (g) X. N. Cheng, W. Xue, J. H. Huang and X. M. Chen, *Dalton Trans.*, 2009, 5701.

27 X.-T. Wang, X.-H. Wang, Z.-M. Wang and S. Gao, *Inorg. Chem.*, 2009, **48**, 1301.

28 (a) E.-Q. Gao, A.-L. Cheng, Y.-X. Xu, M.-Y. He and C.-H. Yan, *Inorg. Chem.*, 2005, **44**, 8822; (b) J. Boonmak, M. Nakano, N. Chaichit, C. Pakawatchai and S. Youngme, *Inorg. Chem.*, 2011, **50**, 7324; (b) X.-Y. Wang, L. Wang, Z.-M. Wang and S. Gao, *J. Am. Chem. Soc.*, 2006, **128**, 674.

29 R. H. Fenton, *Synlett,* **1999,** *8*, 1203.

30 O. V. Dolomanov, L. J. Bourhis, R. J. Gildea, J. A. K. Howard and H. Puschmann, *J. Appl. Cryst*. **2009**, *42*, 339.

31 L. N. Mulay, E. A. Boudreaux, *Theory and Applications of Molecular Diamagnetism*, Wiley-VCH, New York, 1976, p. 491.

Table 1. Crystallographic Data for **1·Cu**, **2·Mn** and **3·Co**

	1·Cu	**2·Mn**	**3·Co**
Formula	$C_{11}H_7CuN_9$	$C_{11}H_7MnN_9$	$C_{11}H_7CoN_9$
fw	328.81	320.20	973.62
Crystal system	Monoclinic	Orthorhombic	Monoclinic
Space group	$P2_1/c$	$Pbca$	$P2_1/c$
a / Å	6.7773(5)	8.9867(7)	10.7778(8)
b / Å	20.7006(16)	14.7912(11)	12.1999(9)
c / Å	8.3965(7)	17.9613(13)	9.5936(7)
α / °	90	90	90
β / °	91.2110(10)	90	106.3912(16)
γ / °	90	90	90
V / Å^3	1177.72(16)	2387.5(3)	1181.84(15)
Z	4	8	4
T / K	150(2)	150(2)	150 (2)
D_c / g cm^{-3}	1.854	1.782	1.822
μ / mm^{-1}	1.864	1.115	1.461
(Δρ)max, min / e Å^{-3}	0.750, -0.859	0.420, -0.331	0.425, -0.330
Measured/independent (R_{int}) reflections	7088/2155(0.0163)	16277/2741(0.0200)	9074/2945(0.0179)
Observed reflections [$I > 2\sigma(I)$]	1997	2616	2670
Goodness-of-fits on F^2	1.109	1.251	1.055
R_1[a], wR_2[b] [$I > 2\sigma(I)$]	0.0406, 0.1213	0.0370, 0.0845	0.0238, 0.0596

[a]$R_1 = (\Sigma||F_O|-|F_C||)/\Sigma|F_O|$, [b]$wR_2 = [\Sigma[w(F_O^2-F_C^2)^2]/\Sigma[w(F_O^2)^2]]^{1/2}$

Table of Contents

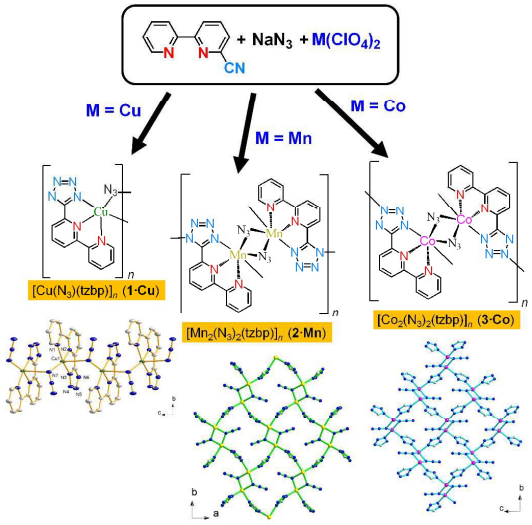

Three new azide-bridged coordination polymers, $[M(N_3)(tzbp)]_n$ (M = Cu, **1·Cu**; Mn, **2·Mn**; Co, **3·Co**), were successfully prepared by introducing a bifunctional tetrazolate/2,2′-bipyridine ligand, 6-(1H-tetrazol-5-yl)-2,2′-bipyridine (Htzbp), from the *in situ* [2+3] cycloaddition of 6-cayno-2,2′-bipyridine in the presence of an excess of sodium azide under hydrothermal conditions.